



## Infrared and THz spectroscopy of nanostructured dielectrics<sup>#</sup>

Jan Petzelt\*

Department of Dielectrics, Institute of Physics, Acad. Sci. Czech Rep., Na Slovance 2, 182 21 Praha 8, Czech Republic

Received 11 May 2009; received in revised form 19 October 2009; accepted 30 October 2009

### Abstract

Results achieved using the infrared/THz spectroscopy of various inhomogeneous dielectrics in the Department of Dielectrics, Institute of Physics, Prague, during the last decade are briefly reviewed. The discussion concerns high-permittivity ceramics with inevitable low-permittivity dead layers along the grain boundaries, relaxor ferroelectrics with highly anisotropic polar nano-regions, classical matrix-type composites, core-shell composites, filled nanoporous glasses, polycrystalline and epitaxial thin films, heterostructures and superlattices on dielectric substrates. The analysis using models based on the effective medium approach is discussed. The importance of depolarizing field and of the percolation of components on the effective ac dielectric response and the excitations contributing to it are emphasized.

**Keywords:** Infrared and THz spectroscopy; Effective medium approximation; Nanostructured ferroelectrics

### I. Introduction

In this review we would like to address briefly the progress achieved within the last decade in quantitative infrared (IR) and time-domain terahertz (THz) spectroscopy of nano-inhomogeneous dielectric materials. The aim is to determine the complex dielectric function of such materials in the  $10^{11}$ – $10^{14}$  Hz range (mainly the polar-phonon range) and broad temperature interval. The response may appreciably differ from that of uniform (homogeneous) components of which the material under study is composed. For achieving this goal, compact and macroscopically homogeneous samples are needed in a plane-parallel form (slab with a diameter typically of 5–10 mm) with a flat polished surface enabling transmission as well as specular (mirror) reflection measurements. For recent more general reviews on results achieved using these techniques and basic definitions see [1,2].

The following types of nanostructured samples have been so far studied in our lab:

1. Dense nano-grain (grain size below 100 nm) or fine-grain (grain size 100–200 nm) ceramics compared with coarse-grain ceramics (grain size  $> 1 \mu\text{m}$ ) and/or single

crystals to study so called dielectric size effect in high-permittivity materials ( $\text{SrTiO}_3$  (STO) [3–5],  $\text{BaTiO}_3$  (BTO) [6],  $(\text{Ba,Sr})\text{TiO}_3$  (BST) [7–9],  $\text{PbMg}_{1/3}\text{Nb}_{2/3}\text{O}_3$ - $\text{PbTiO}_3$  (PMN-PT) solid solution [10];

2. Relaxor ferroelectrics – materials with compositional (chemical) nano-order and/or polar nano-regions (PMN [11–14],  $\text{PbMg}_{1/3}\text{Ta}_{2/3}\text{O}_3$  (PMT) [15],  $\text{Pb}(\text{Zr,Ti})\text{O}_3:\text{La}$  (PLZT) [16–20],  $\text{PbSc}_{1/2}\text{Ta}_{1/2}\text{O}_3$  (PST) [21,22],  $\text{Na}_{1/2}\text{Bi}_{1/2}\text{TiO}_3$  (NBT) [23],  $(\text{Sr,Ba})\text{Nb}_2\text{O}_6$  (SBN) [24] and some others [25–27]);
3. Classical matrix nano-composites – high-permittivity nanoparticles embedded in a low-permittivity matrix (BTO-PVDF) [28];
4. Core-shell composites – compact samples consisting of high-permittivity micron or submicron cores covered with nano-thin shells of another (e.g. low-permittivity) material (BTO-STO, BTO- $\text{BaZrO}_3$  [29], BTO- $\text{Al}_2\text{O}_3$ , BTO- $\text{SiO}_2$  [30]);
5. Nano-porous low-permittivity material filled by a high-permittivity filler (Vycor glass – BTO nano-composite [31]);
6. Polycrystalline and epitaxial thin films of high-permittivity materials; film thickness down to 20 nm (STO [32–40], BTO [41,42], BST [33,43]);
7. Heterostructures – system of several thin films with individual film thicknesses tens of nm (STO- $\text{DyScO}_3$  [39,40,44],  $\text{BST}(x)$ - $\text{BST}(1-x)$  [45]);

<sup>#</sup>Paper presented at 6<sup>th</sup> COST 539 Workshop, Advance Functional Characterization of Nanostructured Materials, February 23–25, 2009, ICMC-CSIC, Madrid, Spain

\* Corresponding author: tel: +420 266 052 166  
fax: +420 286 890 415, e-mail: petzelt@fzu.cz

8. Superlattices – system of several epitaxial layers with nm thicknesses of individual layers and various compositions (BTO-STO) [46].

Most of the samples are studied under quasi-normal reflectance and/or transmittance of the probing IR/THz beam and therefore the following two substantially different evaluation procedures are required. Since the IR/THz beam is transverse, the samples, which are macroscopically uniform in the sample plane (e.g. epitaxial films, heterostructures and superlattices + optically isotropic substrate), can be treated as homogeneous within the probing electric field  $E$  direction and the evaluation of such a multilayer system is performed in a standard way using formulas based on transfer-matrix formalism considering coherent interferences within the individual slabs [47]. In this case the internal macroscopic field is homogeneous in the film plane and no restriction on the thickness of individual slabs in relation to probing wavelength is required. However, if the samples are dielectrically inhomogeneous within the  $E$  direction, depolarization field arises on each interface of different dielectric media, which may strongly influence the resulting effective dielectric response. The averaged (so-called effective) dielectric response strongly depends on the shape and topology of individual homogeneous components and can be calculated only within the framework of some simple models of effective media (Effective Medium Approximation - EMA) [48,49]. EMA models require that the external probing  $E$  is homogeneous within individual components and that the boundaries among all the components are sharp. Moreover, depending on the model used, some simplifying assumptions are made about the shape of components and topology of the composite. The models can be also applied to evaluate the ac dielectric response of individual components, but the condition of  $E$ -homogeneity requires the size of individual components being much smaller than the wavelength of the probing IR wave. This is certainly well fulfilled up to the mid IR range ( $\lambda$  in vacuum  $\geq 10 \mu\text{m}$ , inside the material at least  $\geq 1 \mu\text{m}$ ) if the system under study is nano-inhomogeneous. In strongly absorbing media another condition should be fulfilled: the penetration depth should be also much larger than the component size [50].

The most frequent case of characterizing the effective dielectric function in the IR-THz range in bulk samples is to combine the FTIR reflectivity measurements from opaque (usually  $\sim 1$  mm thick) samples (in the frequency range of strong polar-phonon absorption) with the THz transmittance below the strongly absorbing phonon resonances on thinner plane-parallel samples (appropriate thickness typically from 1 mm in case of transparent samples, down to  $\sim 20 \mu\text{m}$  in case of strongly absorbing samples). Whereas the IR reflectivity should be fitted – usually using the fac-

torized form of the multi-oscillator dielectric function [51] – to evaluate the complex dielectric function from the measured data of the power reflectivity, the THz measurements determine the amplitude as well as the phase of the transmitted (reflected) beam which allows one to calculate the complex dielectric function for each frequency, independently of any model. The reflectivity fits are then combined with the THz dielectric data to obtain a fitted dielectric function for the broad frequency range, typically  $10^{11}$ – $10^{14}$  Hz. In the case of inhomogeneous (two-component) samples, one has to know the dielectric function of at least one of the components and its volume concentration to use an appropriate EMA model for determining the dielectric function of the second component by fitting the effective dielectric function.

In case of supported thin films and heterostructures, the evaluation is performed using the transfer-matrix formalism for the transmission and/or specular reflection from a two- or multi-slab system [38,47]. It turns out to be preferable not to use metallic substrates (electrodes), not only because in this case only the reflection measurements are possible, but also because the sensitivity to the optical parameters of the film is strongly reduced in the range of negative permittivity of the substrate, which is always the case of good conductors in the IR range. So, it is preferable to study films on dielectric substrates and perform transmission measurements using the THz spectroscopy and FTIR spectroscopy in the regions of substrate transparency and perform FTIR reflectance measurements in the regions of substrate opacity. Of course, to be able to evaluate the dielectric function of the film, the optical parameters of the bare substrate and thicknesses of all slabs should be always determined independently. In the case of layered heterostructures, only an effective dielectric function of the whole layered system can be determined, which in this case is a simple arithmetic average of the dielectric functions of individual layers weighted by their volume concentrations (geometry of parallel capacitors). Finally, in the case of superlattices, the thicknesses of individual layers are so small that the mutual coupling of adjacent layers may become important and may influence their individual dielectric functions. But these studies are in the very preliminary state and no relevant data have been so far published.

## II. EMA models

EMA models for dielectric properties of heterostructures have a long and rich history starting from the time of J. C. Maxwell [52]. However, not so much attention was paid to understand the effective ac dielectric response up to the IR range [53]. The most popular model is the EMA model by Bruggeman [54], assuming spherical particles of both components with the di-

electric functions  $\varepsilon_1, \varepsilon_2$  of volume concentrations  $x_1$  and  $x_2$  embedded into the effective medium with the dielectric function  $\varepsilon_{eff}$ :

$$x_2 \frac{\varepsilon_1 - \varepsilon_{eff}}{\varepsilon_1 + 2\varepsilon_{eff}} + x_1 \frac{\varepsilon_2 - \varepsilon_{eff}}{\varepsilon_2 + 2\varepsilon_{eff}} = 0 \quad (1)$$

This model (symmetric in both components) can be used for any volume concentration. However, the basic progress was achieved later by Bergman [55] who proved that the effective response of any two-component composite with dielectric functions  $\varepsilon_1$  and  $\varepsilon_2$  of volume concentrations  $x_1$  and  $x_2$  within the EMA can be separated into additive parts:

$$\varepsilon_{eff} = \varepsilon_1 V_1(x_1) + \varepsilon_2 V_2(x_2) + \int_0^1 \frac{x_1}{(1-n)} G(n, x_1) \frac{\varepsilon_1 \varepsilon_2}{(1-n)\varepsilon_2 + n\varepsilon_1} dn \quad (2)$$

The first two terms on the right-hand side describe the original responses just weighted by factors  $0 \leq V_1 \leq x_1$  and  $0 \leq V_2 \leq x_2$ . This part is not influenced by the depolarizing field and corresponds therefore to the volume part which is macroscopically percolated in the direction of  $E$  [49]. The third integral term describes the response of the remaining part which is influenced in various manners by the depolarizing field. The so-called spectral function  $G(n)$  characterizes the geometry, topology and interactions of individual homogeneous components and  $0 \leq n \leq 1$  is the generalized depolarizing factor. It can be shown [49] that all concrete solvable EMA models or acceptable empirical mixing formulas correspond to a particular choice of  $G, V_1$  and  $V_2$ .

The particular advantage of separating the percolated and non-percolated part of the effective dielectric response becomes evident when discussing the ac response. Generally, the ac response consists of several resonance and relaxation dispersion regions in the spectrum (resonances are mostly due to polar phonon modes in the IR, relaxations at lower frequencies appear in impure, inhomogeneous, disordered and/or strongly anharmonic systems), which are characterized by poles of the complex permittivity in the complex frequency plane. In the percolated part of the response the frequencies of these poles remain unchanged so that all dispersion regions in the ac response remain un-shifted, just weaker by the factor of  $V_1$  or  $V_2$ . The non-percolated part of the response is, however, influenced by the depolarizing field in such a way that all dispersion regions in the response are somehow shifted, which accounts for the modified effective static response [56]. Particularly, if high-permittivity particles are embedded into a lower-permittivity matrix, the dispersion frequencies of the particles are shifted up, resulting in a reduced ef-

fective static permittivity. These up-shifts are the greater the stronger are the dielectric strengths (contributions to the static permittivity) of the dispersion in question. For instance, in a paraelectric ceramic, softening of the strong ferroelectric soft mode or slowing down of a critical relaxation is blocked if the shells have low permittivity (so called dead or passive layers), and the Curie-Weiss law is therefore strongly modified [57] (Curie temperature shifted down and the permittivity anomaly at the ferroelectric transition reduced). Therefore in porous and powdered samples no mode softening can be observed (the softening is just blocked by the depolarizing field on the particle surfaces, if the contact among particles is not macroscopically percolated), even if the ferroelectric transition takes place. Therefore it is quite difficult to determine the ferroelectric transition temperature  $T_c$  and discuss its size effect in such samples.

The Bergman representation is also very useful in the case of granular materials or core-shell composites with 0-3 connectivity. In this case it is clear that the cores are not percolated at all ( $V_1 = 0$ ), and if the shell volume is small,  $x_2 \ll x_1$ , the function  $G(n)$  in a good approximation is nonzero only for one value of  $n$ . This results into so-called generalized brick-wall model [58], valid for almost arbitrary shape and topology of the cores with thin shells:

$$\varepsilon_{eff} = \varepsilon_2 \left(1 - \frac{x_1}{1-n}\right) + \frac{x_1}{1-n} \frac{\varepsilon_1 \varepsilon_2}{(1-n)\varepsilon_2 + n\varepsilon_1} \quad (3)$$

It contains just one free parameter  $n$ , characterizing the particle shape and topology. For  $n = (1/3)x_2$  ( $x_2 = 1-x_1$ ), the frequently used brick-wall (brick-layer) model with cubic bricks and the coated-spheres model (Hashin-Shtrikman [59]) are recovered, both latter models being equivalent in the limit of small  $x_2$  [58]:

$$\varepsilon_{eff} = \varepsilon_2 + \frac{3x_1 \varepsilon_2 (\varepsilon_1 - \varepsilon_2)}{3\varepsilon_2 + x_2 (\varepsilon_1 - \varepsilon_2)} \quad (4)$$

Within this model under some assumptions (small  $\tan \delta \ll 1$  for both components,  $\varepsilon_1 \gg \varepsilon_2$ ) also the effective loss tangent  $\tan \delta = \varepsilon''/\varepsilon'$  of a core-shell composite was calculated [29] and in the limit of small  $x_2$  a simple approximate relation was derived:

$$\frac{\tan \delta_{eff}}{\varepsilon_{eff}'} \approx \frac{\tan \delta_1}{\varepsilon_1'} \quad (5)$$

Therefore the effective loss factor in a core-shell composite decreases roughly proportionally to its effective permittivity. So, both the effective permittivity and loss tangent could be strongly reduced in a core-shell composite with a small shell permittivity, however, their ratio remains approximately constant. In [29] also

the electric-field tunability was calculated with the conclusion that the field change of the loss tangent should be stronger in the composite than in the core material.

Another important case, where the EMA can be used, concern polycrystalline ceramics, films or composites in which the individual crystal grains are anisotropic. Stroud [60] has shown that such systems are equivalent to a composite of isotropic particles whose dielectric responses are equal to principle dielectric responses of the anisotropic crystallite. For instance, a dense and macroscopically isotropic polycrystal comprised of dielectrically uniaxial crystallites of arbitrary shapes is equivalent to a two-component composite of isotropic particles (of possibly different shape and topology) with the corresponding two principle dielectric responses and with the volume concentration of 1/3 and 2/3 for the extraordinary and ordinary response, respectively. Such approach was first successfully used for fitting the IR reflectivity of non-ferroelectric optically uniaxial pressed pellets with various particle shapes [61]. Here the concept of percolation is not so straightforward and our experience shows that in this case the Lichtenecker model [62] rather than the Bruggeman EMA yields better results:

$$\varepsilon_{eff}^{\alpha} = (1-x)\varepsilon_1^{\alpha} + x\varepsilon_2^{\alpha}, \quad -1 \leq \alpha \leq 1 \quad (6)$$

This formula was originally suggested as purely empirical, but recently it has been demonstrated that it corresponds to some particular (for general  $\alpha$  rather complex) topologies [63] and its spectral function was calculated [64]. By varying the exponent  $\alpha$  it passes from parallel plate-capacitor geometry ( $\alpha = 1$ ) with no depolarizing field and complete percolation of both components over  $\alpha = 0$ , which represents the logarithmic law with uniform distribution of all depolarizing factors and percolation threshold of both components independently of the concentration  $x$ , to series plate-capacitor geometry ( $\alpha = -1$ ) with maximum depolarizing field and no percolation of any component at all. For  $\alpha$  positive, both components are (partially) percolated and for  $\alpha$  negative neither of the components is percolated, in all cases independently of  $x$ . According to our experience it appears that the case  $\alpha \approx 0$  is most suitable for the ceramics with anisotropic grains.

### III. Dielectric size effect in nano-ceramics

The dielectric size effect, i.e. suppression of the permittivity with the decreasing grain size, is a general and very pronounced phenomenon in all high-permittivity ceramics studied. Two different mechanisms or their combination could be responsible for it:

1. Intrinsic confinement effect of some excitations contributing to the permittivity;
2. Extrinsic effect due to a low-permittivity dead (passive) layer at the grain boundaries.

The first mechanism appears to dominate in relaxor ferroelectrics, as very recently analyzed for PMN-35%PT [10], close to the morphotropic phase boundary. In relaxor ferroelectrics, the dominating contribution to permittivity and its pronounced temperature maximum stems from the dynamics of polar nano-clusters (mainly its breathing, i.e. fluctuations of the cluster boundaries) and is revealed as a broad and strongly temperature dependent relaxation below the polar phonon range. In a fine-grain ( $\sim 150$  nm) PMN-PT ceramics, the relaxations are weaker and shifted to higher frequencies without any critical slowing down near the ferroelectric transition, resulting in about three-times reduced permittivity maximum compared with coarse-grain ( $\sim 4$   $\mu$ m) ceramics fabricated from the same powder. In Ref. [10] it was shown that the effect cannot be fully accounted for by a dead grain-boundary layer and should be understood as predominantly due to pinning of polar nanoclusters by the grain boundaries. It is interesting to note that no appreciable size effect was observed for polar phonon excitations above  $10^{11}$  Hz, which contributed up to about 10% to the maximum permittivity value in the coarse-grain ceramics ( $\sim 17,000$  at 100 Hz). This is, nevertheless, compatible also with the expectation from the dead layers and EMA.

The size effect due to the dead layers appears to dominate in all materials where the soft phonon modes are responsible for the high permittivity. We have proven it for STO and BTO ceramics [3,4,6] and very recently also for BST-0.6 [65]. More quantitative conclusions about the properties and microscopic origin of the dead layers were analyzed only for STO [3,4]. In Fig. 1 the grain-size dependence of the low-frequency permittivity and soft mode frequency are plotted as a function of temperature and compared with the single crystal data on the soft-mode frequency from hyper-Raman scattering [66] and THz spectroscopy [67]. Single-crystal data below the structural transition at 105 K are averaged to avoid the crystal anisotropy in the tetragonal phase. It was shown that the dead layers have surprisingly universal properties independent of grain-size and temperature. They consist of a very thin ( $\sim 1$  nm) and locally very low permittivity layer ( $\varepsilon \approx 10$ ) due to a defect structure of the grain boundary, obviously lacking oxygen (about one O<sup>-</sup>-ion per unit cell). Since the missing charge should be compensated apparently by defect charges diffusing towards the grain boundary during the sintering, dipolar layers out of these charges are created along the grain boundaries, producing in this way effectively polar grain boundaries. Polar grain boundaries in STO were suggested by us already earlier from the appearance of forbidden IR modes in the Raman spectra [68]. These secondary dead layers from both sides of the grain boundaries are thicker ( $\sim 3$  nm) but, unlike the grain boundary itself, they have already perovskite

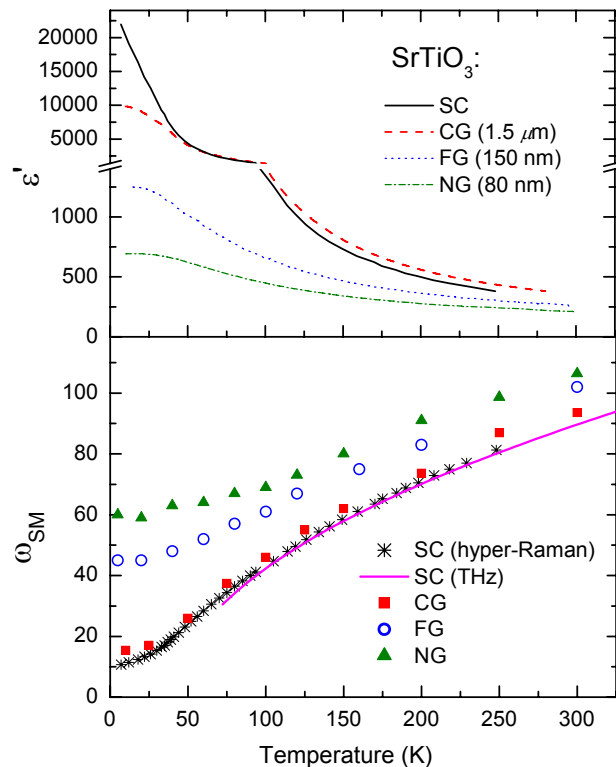


**Figure 1.** Dielectric grain-size effect of the low-frequency permittivity in STO ceramics and temperature dependence of the effective soft-mode frequency (see [3,4]) compared to the behaviour of single crystals SC (see [66,67]). Three ceramics with the mean grain size of 1500 nm (CG), 150 nm (FG) and 80 nm (NG) are compared

structure, only slightly distorted by the present space charge and therefore higher local permittivity, but not as high as in the grain bulk, which we assumed not to differ from the STO crystals. Fitting with a spherical core–double-shell model succeeded to explain all the IR, THz and Raman features down to 80 nm grain size, as well as the low-frequency effective permittivity data, which at low temperatures ( $\epsilon \approx 700$ ) yield a reduction by a factor of 30 compared to single crystals (see Fig. 1). Important feature is that in all the ceramics there is no substantial dielectric dispersion below the ferroelectric soft mode range so that the effective soft-mode hardening is fully responsible for the dielectric size effect. Essentially the same feature was established also in the case of BTO ceramics down to  $\sim 50$  nm grain size [6] and for BST-0.6 ceramics down to  $\sim 150$  nm grain size [65].

#### IV. Relaxor ferroelectrics

From the mesoscopic point of view, relaxor ferroelectrics (shortly relaxors) are characterized by polar nano-regions (PNR), better called polar nano-clusters, because at usual temperatures of their investigation (from the permittivity maximum up to so called Burns temperature  $T_B$ , below which PNR appear) they are rapidly fluctuating. Their size of the order of several nm slightly increases on cooling and saturates in the order of tens of nm at low temperatures. Their dynamics below the polar phonon range was studied in several relaxor materials using audio-frequency, radio-fre-

quency, MW and THz dielectric spectroscopy: PMN [14], PMN-PT [10], PMT [15], PST [22,69], PLZT [16,17], PZN-PMN-PSN [27], NBT [23] and was generally described in [70,71]. Summarizing, below  $T_B$  the PNR emerge from the broad soft-central mode response below the THz range like a Debye relaxation, which softens and broadens on further cooling. Often it also splits into two broad (overlapping) components. The softening of the broad loss peak continues according to the Vogel-Fulcher law down to about the maximum permittivity temperature with the Vogel-Fulcher temperature slightly below it, corresponding to the PNR freezing temperature. Below the freezing temperature, distribution of relaxation frequencies becomes much broader than the range of measurements, resulting in frequency-independent loss (so-called  $1/f$  noise) and logarithmic dispersion of the permittivity, and can be assigned to fluctuations of the PNR boundaries (which may be quite diffuse) over energy barriers with a broad distribution of activation energies [17].

From the point of view of polar phonon physics, the PNR are quasistatic and for the analysis of their dielectric response in the  $10^{11}$ – $10^{13}$  range the EMA models could be used, in a similar way as in ceramics with anisotropic grains [61]. This was for the first time suggested in [11] for PMN and short after discussed for several other relaxors [12]. Later it was used also for evaluation and polar mode assignment in PLZT [19,20]. The main result is that the PNR are generally quite strongly anisotropic,

the local permittivity along their dipole moment being much smaller than that perpendicularly to it. It is caused mainly by a strong splitting of the local soft mode into the  $A_1$  (parallel to local  $P_s$ ) and E component (perpendicular to local  $P_s$ ) below  $T_B$ . The E-component remains quite soft (typically at 1 THz) and overdamped down to low temperatures and in most of inelastic scattering experiments it was so far not resolved from the central peak. But in the dielectric spectra it clearly separates from the PNR relaxation dispersion below  $T_B$  and stays in the THz range down to cryogenic temperatures.

## V. Matrix nano-composites

Recently, attempts in the literature have appeared to study the ferroelectric size effect e.g. in BTO-polymer nano-composites. It was tempting to assign the low-frequency permittivity maximum in such systems to the (shifted) ferroelectric Curie point and interpret it as a size effect of the ferroelectric transition temperature. We have studied the BTO–PVDF polymer composites out of the BTO powder prepared by mechanosynthesis with the mean BTO particles size of  $\sim 7$  nm [28]. Several samples with various thicknesses and BTO-concentrations were studied, to cover the MW, THz and IR range. The effective permittivity in the MW-THz range remains rather small (of the order of 10) and temperature independent. The ferroelectric soft-mode response is strongly broadened and shifted to much higher IR range of 200–400  $\text{cm}^{-1}$  and remains essentially temperature independent, as expected also from the EMA modeling. The dielectric dispersion and its temperature dependence observed below the MHz range [72] is connected with the dispersion in PVDF polymer and presumably with partial interdiffusion of BTO particles into the PVDF matrix. So, no conclusion about the presence of ferroelectricity in the BTO particles and its size effect can be drawn from the dielectric behaviour.

## VI. Core-shell composites

Core-shell composites in a form of dense ceramics are presently a subject of interest with the hope to improve/modify the dielectric properties. For instance, as was mentioned in Sect. 2, in the case of high-permittivity core and low-permittivity and low-loss shell, the effective  $\tan\delta$  is expected to decrease compared to that in the core [29], which could be of interest for MW applications [73]. Our recent studies [29,30] concern several dense core-shell composites with BTO cores of size  $\sim 500$  or  $\sim 200$  nm and the shell thicknesses up to 10 nm, prepared in other labs, mostly by spark plasma sintering [74,75]. In [29]  $\text{BaZr}_{0.2}\text{Ti}_{0.8}\text{O}_3$ ,  $\text{BaZr}_{0.4}\text{Ti}_{0.6}\text{O}_3$ ,  $\text{Ba}_{0.66}\text{Sr}_{0.34}\text{TiO}_3$  and  $\text{Ba}_{0.45}\text{Sr}_{0.55}\text{TiO}_3$  core-shell compositions were studied in a broad temperature range of 10–900 K using THz transmission and FTIR reflectivity measurements. In all the samples, temperature dependence of the THz permittivity differs remarkably from

that at low frequencies and a strong dielectric dispersion and absorption was revealed in THz-MW range, not expected from the EMA modeling. Similar effects were also observed in  $\text{BTO@Al}_2\text{O}_3$  and  $\text{BTO@SiO}_2$  core-shell composites [30]. We assign this feature to interdiffusion of BTO cores into the shells (detected also by electron microscopy [74]), forming in this way a composite with a graded structure rather than with sharp boundaries between the components, as assumed in all EMA models. Unfortunately, no quantitative modeling of these high-frequency features is presently available.

## VII. Vycor glass – BT nano-composite

Recently we succeeded to prepare also a composite of nano-porous Vycor glass filled up with BTO, prepared by sol-gel technique. Vycor glass consists of  $\text{SiO}_2$  matrix with percolated pores of 4–7 nm diameter and  $\sim 30$  nm length and total volume concentration 28%, which by repeated soaking and annealing up to 600°C enabled us to fill up the pores up to 42%. The XRD could not detect any crystal structure, however, the room-temperature IR and THz spectra have shown smeared absorption features in the range of 100, 350 and 550  $\text{cm}^{-1}$ , corresponding presumably to the shifted  $E(\text{TO}1)$ ,  $A_1(\text{TO}1)$  and  $\text{TO}4$  phonon modes of the tetragonal BTO [12]. However, the sharp but weak  $\text{TO}2$  mode near 180  $\text{cm}^{-1}$  was not detected. The latter mode in BTO crystals corresponds to external vibrations of Ba against the  $\text{TiO}_6$  octahedra (so-called Last mode), whereas the three former modes are internal modes of  $\text{TiO}_6$  octahedra, but with displaced Ti ions as in the tetragonal BTO phase, indicated by the large splitting between the E and  $A_1$   $\text{TO}1$  modes. To check if the BTO phase is crystalline or amorphous, we annealed the sample once more to higher temperature ( $\sim 800^\circ\text{C}$ ), but this was connected with a reaction of BTO with the  $\text{SiO}_2$  matrix and forming of new compounds with substantial modification of the XRD and IR spectra. So it seems that our IR spectra of the less annealed sample still indicated at least local ferroelectric phase of BTO (deformed  $\text{TiO}_6$  octahedra with displaced Ti ions) in the nano-pores, even if the XRD was not able to detect any crystallinity. Further studies are in progress to reach any definite conclusion.

## VIII. Heterostructures and superlattices

Our lab was the first place where the ferroelectric soft modes studies in thin films have been started using the FTIR spectroscopy [76]. We were also the first to reveal that in a polycrystalline STO film (PLD on sapphire substrate) the  $\text{TO}1$  soft mode by far does not soften as much as in single crystals or ceramics [77]. Similar pronounced effect was later rediscovered using far IR ellipsometry by Sirenko et al. [78], but its possible explanation was suggested only later by us [32], where it was shown that nano-cracks along some of grain boundaries

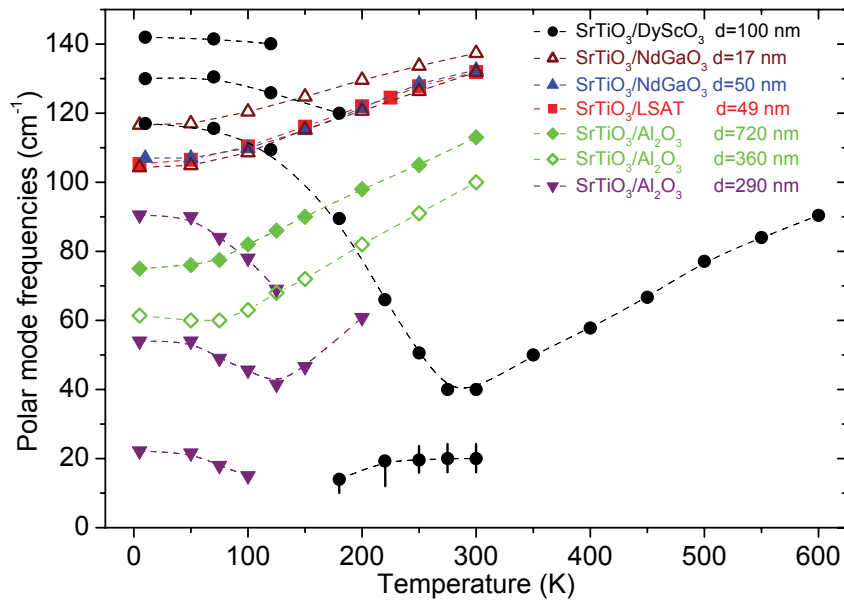


Figure 2. Soft mode behaviour in different STO thin films studied (see [32,36,37,80])

may play a pronounced role even if their volume concentration seems to be negligible (in the order of 0.1%). In polycrystalline films, of course, also the dead layers at grain boundaries play a similar role as in ceramics with comparable grain size, which in films is typically in the 100 nm or even smaller range.

Strain from the substrate (appearing due to different thermal expansion or lattice parameter of the substrate) can influence substantially the phase diagram of STO films particularly in the case of epitaxial films and can induce the ferroelectric phase: up to  $\sim 120$  K (MOCVD film on a (0001) sapphire substrate [32]) or even up to the room temperature (MBE 1% tensile strained film on a DyScO<sub>3</sub> substrate [79]). In our lab we studied THz spectroscopy on similar films and heterostructures including its electric-field tunability [38,40,80]. The soft-mode behaviour in such films on a DyScO<sub>3</sub> substrate confirmed the ferroelectric transition close to the room temperature. In Fig. 2 we have compared the temperature dependences of the soft-mode frequency in this film with the soft-mode frequency behaviour in other films studied by us. Note the very large differences among the various films, particularly at low temperatures. The low-temperature splitting into three components observed in two of the films is interpreted as due to appearance of the ferroelectric and antiferrodistortive transition, which allows the IR activation of the structural soft-mode doublet folded from the Brillouin-zone boundary (well-known from the Raman data on single crystals). In our lab, also the THz tunability of STO films up to room temperature was demonstrated for the first time [38] with the same tunability value as in the MW range and it was shown that it is fully caused by the  $E$ -field dependence of the soft mode. We have demonstrated that the complete in-plane polarized polar-phonon spectra in STO films on various

IR-opaque but dielectric substrates could be well studied by specular FTIR reflection down to thicknesses of  $\sim 20$  nm [36,37]. All the polar phonon frequencies have been found quite sensitive to the strain in the film, but only the soft mode was moreover strongly temperature dependent.

As seen from Fig. 2, we attempted also studying the phonons and ferroelectric transitions in compressed (in-plane) STO films, in which the appearance of the ferroelectric phase was also predicted, but, unlike in tensile films, with  $P_s$  tending perpendicular to the film plane. We studied epitaxial PLD films on NdGaO<sub>3</sub> (-1% compressive strain) [36,80] and on LSAT (La<sub>0.18</sub>Sr<sub>0.82</sub>Al<sub>0.59</sub>Ta<sub>0.41</sub>O<sub>3</sub>) substrate (-0.9% compressive strain) [37]. All the phonons were appreciably stiffened, since the expected ferroelectric instability should have appeared only out of the film plane. In [36] we have suggested (through an appearance of a weak feature in our spectra near 318 cm<sup>-1</sup>, assigned to the silent F<sub>2u</sub> mode, IR activated in the ferroelectric phase) that our film undergoes an out-of-plane ferroelectric transition near 150 K. However, no similar effect has been seen in the film on the LSAT substrate [37]. Our subsequent studies of a new film on the NdGaO<sub>3</sub> substrate have shown [81] that our previously observed feature [36] was an artifact caused by the IR-anisotropic orthorhombic substrate studied in the reflection mode using unpolarized IR light. So, the presence of the ferroelectric transition with out-of-plane  $P_s$  in STO films is still open to further studies.

The BTO and BST films were frequently studied by Raman scattering (see the review by Tenne and Xi in [82]), but not so much by IR spectroscopy [33,41–43,45]. The main reason is that, as in single crystals, the soft mode is overdamped and no pronounced changes near the ferroelectric transitions are seen. It appears that all the ferroelectric transitions on both polycrystal-

line and quasi-epitaxial BTO films on sapphire or MgO are diffuse with some coexistence of phases down to low temperatures. No IR measurements on single-domain epitaxial films are available.

### IX. Heterostructures and superlattices

Recently, also THz and IR studies on multilayers have been started in our lab. Very interesting results, including the  $E$ -field tunability, were obtained from THz spectroscopy of several STO/DyScO<sub>3</sub> multilayers differing by the number of repeating STO/DyScO<sub>3</sub> bilayers and their thicknesses (10–100 nm) with the total film thickness up to 200 nm on the DyScO<sub>3</sub> substrate [40,44]. The tensile stress in STO films induces ferroelectric transition which results in strong soft-mode softening at room temperature (being close to  $T_C$ , but still in the paraelectric phase) compared to bulk crystal and appearance of a central-mode-like relaxation below the THz range coupled to it (see it also in Fig. 2). Under the  $E$ -field, strong stiffening of the soft mode was observed. The enhanced soft-mode damping indicates a gradient in the STO film strain across the multilayer. A very simple model of coupled oscillator (soft mode) and Debye relaxation (central mode), in which only the bare oscillator frequency and damping differ for different samples and fields, describes surprisingly well all the data.

Another set of samples concerned four epitaxial PLD films with a total thickness of 500 nm each: single BST-0.75 layer, single BST-0.25 layer, BST-0.75+BST-0.25 bi-layer and BST-0.25+BST-0.75 bi-layer (each 250 nm thick) on the MgO substrate. Concerning the induced strains, the third sample has the best quality since the lattice mismatch between all the layers including substrate is  $\sim 1.2\%$ . It is known that in BST only the tensile stress in the field direction increases the permittivity, compressive strain reduces it. Our FTIR measurements confirmed that the samples differed appreciably by their phonon spectra, the third sample (substrate+BST-0.75+BST-0.25) giving the largest contribution to the static permittivity [45].

Finally, also FTIR reflectance studies of several high-quality BTO-STO superlattices with the layer thicknesses below 10 unit cells (total thickness  $\sim 100$  nm) on DyScO<sub>3</sub> substrates are in progress [46]. In this case the effective in-plane dielectric response of the whole superlattice can be evaluated and compared with the BST films of the same integral composition and thickness. It should be taken into account that the responses of individual layers form parallel capacitors so that the effective response is simply an arithmetic mean value of both components. In this geometry no activation of new modes from the folded Brillouin zone (seen in Raman spectra [82]) is expected, since the probing  $E$ -field is parallel to the film plane without any depolarizing field effects and with-

out feeling the interfaces between the layers as long as their volume concentration remains small.

### X. Conclusions

We have demonstrated that the IR/THz spectroscopy is a powerful tool for studying dynamic dielectric properties of various inhomogeneous dielectrics. From the spectroscopic data it is possible to evaluate quantitatively the effective dielectric function of any plate-shaped sample and, knowing the topology of individual components, in many cases of two-component samples it is possible to use EMA models for evaluating the dielectric response of one of the components, knowing it for the other one. Moreover, comparing the static effective permittivity extrapolated from the IR response with that directly measured can shed light on the nature of various dielectric anomalies and excitations or mechanisms contributing to the dielectric response.

**Acknowledgement:** The work was supported by the Czech Academy of Sciences (project AVOZ10100520) and by the Czech Ministry of Education (project ME-COST 539). The author would like to thank T. Ostapchuk and D. Nuzhnyy for the figure preparation.

### References

1. J. Petzelt, S. Kamba, J. Hlinka, "Ferroelectric soft modes in ceramics and films", pp. 387–421 in *New Developments in Advanced Functional Ceramics* (Ed. L. Mitoseriu) Transworld Research Network 37/661 (2), Fort P. O., Trivandrum, Kerala, India 2007.
2. J. Petzelt, S. Kamba, "Spectroscopic properties of functional oxide ceramics with pronounced dielectric properties", in *Spectroscopic Properties of Inorganic and Organometallic Compounds: Techniques, Materials and Applications*. Specialist Periodic Report (SPR) (Royal Society of Chemistry), ed. J. Yarwood et al., **40** (2009) 49–71.
3. J. Petzelt, T. Ostapchuk, I. Gregora, D. Nuzhnyy, I. Rychetsky, K. Maca, Z. Shen, "Grain boundary and size effect on the dielectric, infrared and Raman response of SrTiO<sub>3</sub> nanograin ceramics", *Ferroelectrics*, **363** (2008) 227–244.
4. J. Petzelt, T. Ostapchuk, I. Gregora, P. Kuzel, J. Liu, Z. Shen, "Infrared and Raman studies of the dead grain-boundary layers in SrTiO<sub>3</sub> fine-grain ceramics", *J. Phys. Cond. Matter*, **19** (2007) 196222–1/16.
5. J. Petzelt, T. Ostapchuk, I. Gregora, M. Savinov, D. Chvostova, J. Liu, Z. Shen, "Grain boundary effects on dielectric, infrared and Raman response of SrTiO<sub>3</sub> nanograin ceramics". *J. Eur. Ceram. Soc.*, **26** (2006) 2855–2859.
6. T. Ostapchuk, J. Petzelt, M. Savinov, V. Buscaglia, L. Mitoseriu, "Grain-size effect in BaTiO<sub>3</sub> ceramics: study by far infrared spectroscopy", *Phase Transitions*, **79** (2006) 361–374.

7. T. Ostapchuk, M. Savinov, J. Petzelt, A. Pashkin, M. Dressel, E. Smirnova, V. Lemanov, A. Sotnikov, M. Weihnacht, “Far infrared spectroscopy of  $\text{Sr}_{1-x}\text{Ba}_x\text{TiO}_3$  ( $0.01 \leq x \leq 0.2$ ) ceramics”, *Ferroelectrics*, **353** (2007) 70–77.
8. T. Ostapchuk, J. Petzelt, P. Kuzel, S. Veljko, A. Tkach, P. Vilarinho, I. Ponomareva, L. Bellaiche, A. Smirnova, V. Lemanov, A. Sotnikov, Weihnacht, “Infrared and THz soft-mode spectroscopy of  $(\text{Ba,Sr})\text{TiO}_3$  ceramics”, *Ferroelectrics*, **367** (2008) 139–148.
9. T. Ostapchuk et al., to be published.
10. V. Bovtun, S. Kamba, S. Veljko, D. Nuzhnyy, J. Kroupa, M. Savinov, P. Vanek, J. Petzelt, J. Holc, M. Kosec, H. Amorin, M. Alguero, “Broadband dielectric spectroscopy of phonons and polar nanoclusters in  $\text{PbMg}_{1/3}\text{Nb}_{2/3}\text{O}_3$ -35% $\text{PbTiO}_3$  ceramics: Grain size effects”, *Phys. Rev. B* **79** (2009) 104111–1/12.
11. J. Hlinka, T. Ostapchuk, D. Noujni, K. Kamba, J. Petzelt, “Anisotropic dielectric function in polar nanoregions of relaxor ferroelectrics”, *Phys. Rev. Lett.* **96** (2006) 027601–1/4.
12. J. Hlinka, J. Petzelt, S. Kamba, D. Noujni, T. Ostapchuk, “Infrared dielectric response of relaxor ferroelectrics”. *Phase Transitions*, **79** (2006) 41–78.
13. S. Kamba, M. Kempa, V. Bovtun, J. Petzelt, K. Brinkman, N. Setter, “Soft and central mode behavior in  $\text{PbMg}_{1/3}\text{Nb}_{2/3}\text{O}_3$  relaxor ferroelectric”, *J. Phys. Condens. Matter*, **17** (2005) 3965–3974.
14. V. Bovtun, S. Veljko, S. Kamba, J. Petzelt, S. Vakhruhev, Y. Yakimenko, K. Brinkman, N. Setter, “Broadband dielectric response of  $\text{PbMg}_{1/3}\text{Nb}_{2/3}\text{O}_3$  relaxor ferroelectrics: single crystals, ceramics and thin films”, *J. Eur. Ceram. Soc.*, **26** (2006) 2867–2875.
15. S. Kamba, D. Nuzhnyy, S. Veljko, V. Bovtun, J. Petzelt, Y.L. Wang, N. Setter, J. Levoska, M. Tyunina, J. Macutkevic, J. Banys, “Dielectric relaxation and polar phonon softening in relaxor ferroelectric  $\text{PbMg}_{1/3}\text{Ta}_{2/3}\text{O}_3$ ”, *J. Appl. Phys.*, **102** (2007) 074106–1/9.
16. S. Kamba, V. Bovtun, J. Petzelt, I. Rychetsky, R. Mizaras, A. Brilingas, J. Banys, J. Grigas, M. Kosec, “Dielectric dispersion of the PLZT ceramics in the frequency range 10 Hz–100 THz”, *J. Phys.: Cond. Matter*, **12** (2000) 497–519.
17. I. Rychetsky, S. Kamba, V. Porokhonsky, A. Pashkin, M. Savinov, V. Bovtun, J. Petzelt, M. Kosec, M. Dressel, “Frequency-independent dielectric loss ( $1/f$  noise) in PLZT relaxors at low temperatures”, *J. Phys. Condens. Matter*, **15** (2003) 6017–6030.
18. S. Kamba, D. Nuzhnyy, O. Tkac, B. Malic, M. Kosec, J. Petzelt, “High-temperature soft phonon behaviour in PLZT 8/65/35 relaxor ferroelectrics”, *Phase Transitions*, **81** (2008) 1005–1012.
19. E. Buixaderas, I. Gregora, S. Kamba, J. Petzelt, M. Kosec, “Raman spectroscopy and effective dielectric function in PLZTx/40/60”, *J. Phys. Cond. Matter*, **20** (2008) 345229–1/10.
20. E. Buixaderas, S. Kamba, J. Petzelt, J. Drahoukoupil, F. Laufek, M. Kosec, “Dielectric anisotropy in relaxor ferroelectric  $\text{Pb}_{0.775}\text{La}_{0.15}(\text{Zr}_{0.4}\text{Ti}_{0.6})\text{O}_3$  ceramics”, *Appl. Phys. Letters*, **91** (2007) 112909–1/3.
21. J. Petzelt, E. Buixaderas, A. Pronin, “Infrared dielectric response of ordered and disordered ferroelectric  $\text{Pb}(\text{Sc}_{1/1}\text{Ta}_{1/2})\text{O}_3$  ceramics”, *Mater. Sci. Eng. B* **55** (1998) 86–94.
22. S. Kamba, M. Berta, M. Kempa, J. Hlinka, J. Petzelt, K. Brinkman, N. Setter, “Far-infrared soft-mode behavior in  $\text{PbSc}_{1/2}\text{Ta}_{1/2}\text{O}_3$  thin films”, *J. Appl. Phys.*, **98** (2005) 074103–1/6.
23. J. Petzelt, S. Kamba, J. Fabry, D. Noujni, V. Porokhonsky, A. Pashkin, I. Franke, K. Roleder, J. Suchanicz, R. Klein, G.E. Kugel, “Infrared, Raman and high-frequency dielectric spectroscopy and the phase transitions in  $\text{Na}_{1/2}\text{Bi}_{1/2}\text{TiO}_3$ ”, *J. Phys. Condens. Matter*, **16** (2004) 2719–2731.
24. E. Buixaderas, M. Savinov, M. Kempa, S. Veljko, S. Kamba, J. Petzelt, R. Pankrath, S. Kapphan, “Infrared and dielectric spectroscopy of the relaxor ferroelectric  $\text{Sr}_{0.61}\text{Ba}_{0.39}\text{Nb}_2\text{O}_6$ ”, *J. Phys. Condens. Matter*, **17** (2005) 653–666.
25. S. Kamba, S. Veljko, M. Kempa, M. Savinov, V. Bovtun, P. Vanek, J. Petzelt, M. Stennett, I. Reaney, A.R. West, “Dielectric spectra of a new relaxor ferroelectric system  $\text{Ba}_2\text{LnTi}_2\text{Nb}_3\text{O}_{15}$  (Ln=La, Nd)”, *J. Eur. Ceram. Soc.*, **25** (2005) 3069–3073.
26. V. Bovtun, S. Kamba, S. Veljko, D. Nuzhnyy, K. Knížek, M. Savinov, J. Petzelt, “Relaxor-like behavior of a new lead-free tetragonal tungsten bronze  $\text{Sr}_2\text{LaTi}_2\text{Nb}_3\text{O}_{15}$  ceramics”, *J. Appl. Phys.*, **101** (2007) 054115–1/6.
27. J. Macutkevic, S. Kamba, J. Banys, A. Brilingas, A. Pashkin, J. Petzelt, K. Bormanis, A. Sternberg: “Infrared and broadband dielectric spectroscopy of PZN-PMN-PSN relaxor ferroelectrics: Origin of two-component relaxation”, *Phys. Rev. B* **74** (2006) 104106–1/10.
28. D. Nuzhnyy, J. Petzelt, I. Rychetsky, S. Veljko, J. Kulek, B. Hilczer, “Time-domain terahertz and infrared spectroscopy of  $\text{BaTiO}_3$ -PVDF nanocomposites”, *Phase Transitions*, **81** (2008) 1049–1057.
29. D. Nuzhnyy, J. Petzelt, I. Rychetsky, V. Buscaglia, M.T. Buscaglia, P. Nanni, “THz and IR dielectric response of  $\text{BaTiO}_3$  core-shell composites: evidence for interdiffusion”, *J. Phys. D: Appl. Phys.*, **42** (2009) 155408–1/8.
30. D. Nuzhnyy et al., to be published.
31. D. Nuzhnyy, J. Petzelt, P. Vanek, J. Bursik, “Infrared spectroscopy of  $\text{BaTiO}_3$  confined in nanoporous  $\text{SiO}_2$  Vycor glass”, Abstract for COST 539 Final Workshop, Aveiro, October 28-30 (2009).
32. T. Ostapchuk, J. Petzelt, V. Železný, A. Pashkin, J. Pokorný, I. Drbohlav, R. Kužel, D. Rafaja, B.P. Gorshunov, M. Dressel, Ch. Ohly, S. Hoffmann-Eifert, R. Waser, “Origin of soft-mode stiffening and reduced dielectric response in  $\text{SrTiO}_3$  thin films”. *Phys. Rev. B* **66** (2002) 235406–1/12.

33. J. Petzelt, T. Ostapchuk, A. Pashkin, I Rychetský, “FIR and near-millimetre dielectric response of SrTiO<sub>3</sub>, BaTiO<sub>3</sub> and BST films and ceramics”, *J. Eur. Ceram. Soc.*, **23** (2003) 2627–2632.
34. J. Petzelt, P. Kužel, I. Rychetský, A. Pashkin, T. Ostapchuk, “Dielectric response of soft modes in ferroelectric thin films”, *Ferroelectrics*, **288** (2003) 169–185.
35. J. Petzelt, I. Rychetsky, “Effective dielectric function in high-permittivity ceramics and films”, *Ferroelectrics*, **316** (2005) 89–95.
36. Y. Yamada, J. Petzelt, A.K. Tagantsev, S. Denisov, D. Noujni, P.K. Petrov, A. Mackova, K. Fujito, T. Kiguchi, K. Shinozaki, N. Mizutani, V.O. Sherman, P. Muralt, N. Setter, “In-plane and out-of-plane ferroelectric instabilities in epitaxial SrTiO<sub>3</sub> films”, *Phys. Rev. Lett.*, **96** (2006) 157602.
37. D. Nuzhnyy, J. Petzelt, S. Kamba, T. Yamada, M. Tyunina, A. K. Tagantsev, J. Levoska, N. Setter, “Polar phonons in SrTiO<sub>3</sub> thin films: effect of compressive stress and grain boundaries”, *J. Electroceram.*, **22** (2009) 297–301.
38. P. Kuzel, F. Kadlec, H. Nemeč, R. Ott, E. Hollmann, N. Klein, “Dielectric tunability of SrTiO<sub>3</sub> thin films in the terahertz range”, *Appl. Phys. Lett.*, **88** (2006) 102901–1/3.
39. P. Kuzel, F. Kadlec, J. Petzelt, J. Schubert, G. Panaitov, “Highly tunable SrTiO<sub>3</sub>/DyScO<sub>3</sub> heterostructures for applications in the terahertz range”, *Appl. Phys. Lett.*, **91** (2007) 232911–1/3.
40. P. Kuzel, C. Kadlec, F. Kadlec, J. Schubert, G. Panaitov, “Field-induced soft mode hardening in SrTiO<sub>3</sub>/DyScO<sub>3</sub> multilayers”, *Appl. Phys. Lett.*, **93** (2008) 052910–1/3.
41. T. Ostapchuk, J. Petzelt, J. Pokorný, A. Pashkin, V. Železný, M. Dressel, B. Gorshunov, “Far-infrared and Raman spectroscopy of BaTiO<sub>3</sub> thin films”, *Ferroelectrics*, **303** (2004) 173–175.
42. T. Ostapchuk, J. Pokorný, A. Pashkin, J. Petzelt, V. Zelezny, D. Rafaja, I. Drbohlav, “Soft-mode spectroscopy of BaTiO<sub>3</sub> thin films”, *J. Eur. Ceram. Soc.*, **25** (2005) 3063–3067.
43. E. John, P. Kuzel et al., to be published.
44. C. Kadlec, F. Kadlec, H. Nemeč, P. Kuzel, J. Schubert, G. Panaitov, “High tunability of the soft mode in strained SrTiO<sub>3</sub>/DyScO<sub>3</sub> multilayers”, *J. Phys. Cond. Matter*, **21** (2009) 115902–1/7.
45. E. John, J. Petzelt et al., to be published.
46. V. Zelezny, A. Soukiasian, D.G. Schlom, “Infrared phonon modes in epitaxial BaTiO<sub>3</sub>/SrTiO<sub>3</sub> superlattices”, Abstract book of *Workshop on the Fundamental Physics of Ferroelectrics 2009*, Colonial Williamsburg, USA, February 8–11 (2009).
47. M. Born, E. Wolf, *Principles of Optics*, 7<sup>th</sup> Edition, Cambridge Univ. Press, New York 2003.
48. O. Hudák, I. Rychetský, J. Petzelt, “Dielectric response of microcomposite ferroelectrics”, *Ferroelectrics*, **208-209** (1998) 429–447.
49. I. Rychetský, O. Hudák, J. Petzelt, “Dielectric properties of microcomposite ferroelectrics”, *Phase Transitions*, **67** (1999) 725–739.
50. I. Rychetský, J. Petzelt, “Dielectric properties of ferroelectric powders and micro-composites”, *Ferroelectrics*, **236** (2000) 223–234.
51. E. Buixaderas, S. Kamba, J. Petzelt, “Lattice dynamics and central-mode phenomena in the dielectric response of ferroelectrics and related materials”, *Ferroelectrics*, **308** (2004) 131–192.
52. C. Brosseau, “Modelling and simulation of dielectric heterostructures: a physical survey from a historical perspective”, *J. Phys. D* **39** (2006) 1277–1294.
53. W. Theiss, “The use of effective medium theories in optical spectroscopy” pp. 149–176 in *Advances in Sol. State Phys.*, **33** (Ed. E. Helbig) Vieweg, Braunschweig 1994.
54. D.A.G. Bruggeman, “Berechnung verschiedener physikalischer Konstanten von heterogen Substanzen”, *Ann. Phys. (Leipzig)*, **24** (1935) 636–664.
55. D.J. Bergman, “The dielectric constant of a composite material – a problem in classical physics”, *Phys. Repts.*, **43** (1978) 377–407.
56. J. Petzelt, J. Hlinka, S. Kamba, T. Ostapchuk, D. Noujni, I. Rychetsky, “Effective infrared response of inhomogeneous ferroelectrics”, *Ferroelectrics*, **334** (2006) 199–210.
57. Z. Zhao, V. Buscaglia, M. Viviani, M.T. Buscaglia, L. Mitoseriu, A. Testino, M. Nygren, M. Johnsson, P. Nanni, “Grain-size effects on the ferroelectric behavior of dense nanocrystalline BaTiO<sub>3</sub> ceramics”, *Phys. Rev. B* **70** (2004) 024107–1/8
58. I. Rychetsky, J. Petzelt, “Dielectric spectra of grainy high-permittivity materials”, *Ferroelectrics*, **303** (2004) 137–140.
59. Z. Hashin, S. Shtrikman, “A variational approach to the theory of effective magnetic permeability of multiphase materials”, *J. Appl. Phys.*, **33** (1962) 3125–3131.
60. D. Stroud, “Generalized effective medium approach to the conductivity of an inhomogeneous material”, *Phys. Rev. B* **12** (1975) 3368–3373.
61. C. Pecharroman, J.E. Iglesias, “Effect of the particle shape on the IR reflectance spectra of pressed powders of anisotropic materials”, *Appl. Spectroscopy*, **4** (2000) 634–638.
62. K. Lichtenecker, “Die Dielektrizitätskonstante natürlicher und künstlicher Mischkörper”, *Phys. Z.*, **27** (1926) 115–158.
63. T. Zakri, J.-P. Laurent, M. Vauclin, “Theoretical evidence for Lichtenecker’s mixture formulae based on the effective medium theory” *J. Phys. D: Appl. Phys.*, **31** (1998) 1589–1594.
64. A.V. Goncharenko, V.Z. Lozovski, E.F. Venger, “Lichtenecker’s equation: applicability and limitations”, *Optics Commun.*, **174** (2000) 19–32.
65. T. Ostapchuk et al., to be published.
66. A. Yamanaka, M. Kataoka, Y. Inaba, K. Inoue, B. Hehlen, E. Courtens, “Evidence for competing orderings in strontium titanate from hyper-Raman scattering spectroscopy”, *Europhys. Lett.*, **50**, (2000) 688–694.

67. P. Kuzel, F. Kadlec, “Recent developments in terahertz optoelectronics: Tunable structures and Modulators for THz light”, *C. R. Physique*, **9** (2008) 197–214.
68. J. Petzelt, T. Ostapchuk, I. Gregora, I. Rychetský, S. Hoffmann-Eifert, A.V. Pronin, Y. Yuzyuk, B.P. Gorshunov, S. Kamba, V. Bovtun, J. Pokorný, M. Savinov, V. Porokhonskyy, D. Rafaja, P. Vaněk, A. Almeida, M.R. Chaves, A.A. Volkov, M. Dressel, R. Waser, “Dielectric, infrared and Raman response of undoped SrTiO<sub>3</sub> ceramics: Evidence of polar grain boundaries”, *Phys. Rev.* **B 64** (2001) 184111–1/10.
69. V. Bovtun, V. Porokhonskyy, J. Petzelt, M. Savinov, J. Endal, C. Elissalde, C. Malibert, „Microwave dielectric properties of the ordered and disordered Pb(Sc<sub>1/2</sub>Ta<sub>1/2</sub>)O<sub>3</sub> ceramics”, *Ferroelectrics*, **238** (2000) 581–588
70. V. Bovtun, J. Petzelt, V. Porokhonskyy, S. Kamba, T. Ostapchuk, M. Savinov, P. Samoukhina, P. Vilarinho, J. Baptista, “Dielectric Response of Some Relaxor Ferroelectrics in a Wide Frequency Range” pp. 109–121, in: *Grain Boundary Engineering of Electronic Ceramics-Proceedings of a COST 525 meeting held in Aveiro, Portugal 2001*, British Ceramic Proceedings **63** (Eds. R. Freer., J. Van herle, J. Petzelt, C. Leach), London, Maney Publisher, 2003.
71. V. Bovtun, J. Petzelt, S. Kamba, V. Porokhonskyy, A. Pashkin, S. Veljko, P. Samoukhina, Y. Yakimenko, “High-frequency dielectric spectroscopy of relaxor ferroelectrics and related materials” pp. 757–759 in *MSMW’04 Symposium Proceedings. Kharkov, Ukraine, June 21-26, 2004*, **2**, 2004.
72. J. Kulek, I. Szafraniak, B. Hilczer, M. Polomska, “Dielectric and pyroelectric response of PVDF loaded with BaTiO<sub>3</sub> obtained by mechanosynthesis”, *J. Non-Cryst. Solids*, **353** (2007) 4448–4452.
73. A.K. Tagantsev, V.O. Sherman, K.F. Astafiev, J. Venkatesh, N. Setter, “Ferroelectric materials for microwave tunable application”, *J. Electroceram.*, **11** (2003) 5–66.
74. M.T. Buscaglia, M. Viviani, Z. Zhao, V. Buscaglia, P. Nanni, “Synthesis of BaTiO<sub>3</sub> core-shell particles and fabrication of dielectric ceramics with local graded structure”, *Chem. Mater.*, **18**, (2006) 4002–4010.
75. C. Elissalde, M. Maglione, C. Estournes, “Tailoring dielectric properties of multilayer composites using spark plasma sintering”, *J. Am. Ceram. Soc.*, **90**, (2007) 973–976.
76. I. Fedorov, J. Petzelt, V. Železný, K. Brooks, G.A. Komandin, A.A. Volkov, Y. Huang, N. Sester, “Far infrared dielectric response of PbTiO<sub>3</sub> and PbZr<sub>1-x</sub>TiO<sub>3</sub> thin ferroelectric films” *J. Phys. Cond. Matter*, **7** (1995) 4313–4323.
77. I. Fedorov, V. Železný, J. Petzelt, V. Trepakov, M. Jelínek, V. Trtík, M. Čerňanský, V. Studnička, “Far-infrared spectroscopy of a SrTiO<sub>3</sub> thin film” *Ferroelectrics*, **208-209** (1998) 413–427.
78. A.A. Sirenko, C. Bernhard, A. Golnik, A.M. Clark, J. Hao, W. Si, X.X. Xi, “Soft-mode hardening in SrTiO<sub>3</sub> thin films”, *Nature*, **404** (2000) 373–376.
79. J.H. Haeni, P. Irvin, W. Chang, R. Uecker, P. Reiche, Y.L. Li, S. Choudhury, W. Tian, M.E. Hawley, B. Craigo, A.K. Tagantsev, X.Q. Pan, S.K. Streiffer, L.Q. Chen, S.W. Kirchoefer, J. Levy, D. G. Schlom, “Room-temperature ferroelectricity in strained SrTiO<sub>3</sub>”, *Nature*, **430**, (2004) 758–761.
80. D. Nuzhnyy, J. Petzelt, S. Kamba, P. Kuzel, C. Kadlec, V. Bovtun, M. Kempa, J. Schubert, C.M. Brooks and D.G. Schlom, “Soft mode behavior in SrTiO<sub>3</sub>/DyScO<sub>3</sub> thin films: Evidence of ferroelectric and antiferrodistortive phase transitions”, *Appl. Phys. Lett.*, *in press*.
81. D. Nuzhnyy et al., to be published.
82. D.A. Tenne, X. Xi, “Raman spectroscopy of ferroelectric thin films and superlattices”, *J. Am. Ceram. Soc.*, **91**, (2008) 1820–1834.